

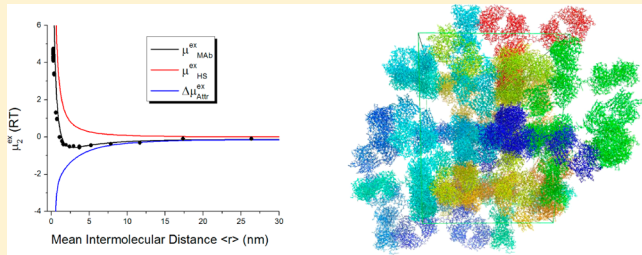
Cosolute Effects on the Chemical Potential and Interactions of an IgG1 Monoclonal Antibody at High Concentrations

Thomas M. Scherer*

Genentech (a Member of the Roche Group), Late Stage Pharmaceutical Development, 1 DNA Way, South San Francisco, California 94080, United States

 Supporting Information

ABSTRACT: The solution thermodynamics and interactions of a reversibly self-associating IgG1 monoclonal antibody have been investigated as a function of cosolute type (NaCl, NaSCN, arginine-HCl) and cosolute concentration over a wide range of protein concentrations (1–235 mg/mL) using static light scattering. The nonideality of mAb solutions is analyzed within the simplifying framework of a two-component system to obtain the dependencies of the excess chemical potential of the mAb on protein and cosolute concentrations. Using hard spheres as a model of mAbs in the absence of intermolecular interactions, the mean interparticle distances can be estimated as a function of antibody concentration. Analysis of MAb1 excess chemical potential and mean intermolecular distance results in a potential function representing the sum of protein–protein interactions and their contributions to solution nonideality. This approach facilitates evaluation of the relative contributions of attractive/repulsive intermolecular interactions and excluded volume effects, as well as the effects of cosolutes on protein multiparticle interactions in crowded conditions. Underlying the dominant effect of volume exclusion at high protein concentrations, attractive interactions were found to be amplified with decreasing intermolecular distances by the MAb1 many-body correlations. Comparison of the cosolute concentration dependence of the protein chemical potential, $d\mu_2^{\text{ex}}/dC_3$, across the mAb concentrations demonstrates that MAb1 self-association is reduced with increasing ionic strength and in a series based on cosolute identity; Arg-Cl > NaSCN > NaCl. The effectiveness of arginine-HCl and NaSCN in modulating MAb1 excess chemical potential in concentrated solutions is ascribed to the cosolute’s ability to mitigate both electrostatic as well as weaker hydrophobic attractive interactions between MAb1 molecules. This investigation presents the first direct analysis of cosolute specific effects on protein–protein interactions at high concentrations, and provides a novel approach for characterizing the many-body effects that contribute to solution nonideality.



INTRODUCTION

Knowledge of protein interactions at high concentrations and the role that cosolutes play in their regulation is not only fundamental to understanding the biological processes governing life, but also important for biopharmaceutical manufacture and product development. The consequences of attractive intermolecular interactions in concentrated (>10–20 mg/mL) solutions of MAbs may manifest as a range of issues such as opalescence, limited solubility, aggregation, elevated viscosity, and uncontrolled phase transitions.^{1–3} It is generally accepted that both specific and nonspecific protein–protein interactions are governed by an array of molecular interaction forces, including electrostatic, van der Waals (dipole interactions), and hydrophobic, as well as the direct interactions with water.⁴ Localized surface features (patches of heterogeneity) are increasingly recognized as contributors to the characteristic differences in protein solution behavior.^{5–8} Protein solution properties and protein–protein interactions therefore appear to be modulated *in vivo* through not only amino acid composition, but also higher order structural features and surface presentation of chemical moieties.

Protein interactions in water are also clearly mediated by the other solution components present. Cosolutes, including the important biological osmolytes sucrose, betaine and trehalose, denaturants such as urea and guanidine, as well as different salts (e.g., “Hofmeister series” salts), are inextricably linked to protein solution behavior as an effective way of tuning the stability and interactions of proteins in solution.^{9–11} Although the modification of solution ionic strength and consequent charge screening by salts is well-known, exactly how cosolute specific effects influence protein solution behavior remains an active area of study. The primary hofmeister series effects of ions are currently believed to occur through direct interactions with the protein rather than modification of the solvent (water) properties. Both anions^{12,13} and cations^{14,15} have been reported to produce the cosolute specific effects of the hofmeister series. Recent insights from solvent accessible surface area analysis¹⁶ and site-specific ion binding to protein surfaces¹⁷ also support a

Received: September 14, 2012

Revised: January 15, 2013

Published: January 18, 2013

more complex interpretation of ion–protein interactions that includes both general interactions with the protein surface (preferential binding/exclusion) and more specific surface residue binding tendencies. Arginine, an amino acid with important biotechnological applications, is recognized as a cosolute with unique effects on the solution behavior of proteins that can be advantageous during protein purification, refolding, and storage.¹⁸ Experimental and *in silico* characterization of arginine solution thermodynamics also suggest a complex balance of preferential binding and exclusion interactions in a protein-specific manner.^{19–21} The net effects of arginine salts in mAb solutions can also offer improvement in the physical stability or reduction of solution viscosities at high mAb concentrations.^{22–24}

Solution light scattering techniques (SAXS, SANS, DLS) and particularly static light scattering (SLS) are powerful tools for the investigation of solution thermodynamics and protein interactions over a wide range of concentrations. Protein interactions in dilute solutions are most often quantified with the osmotic second virial coefficient, which represents the spherically averaged interactions between two molecules as a means to study the effects of ionic strength and salt type on the solution behavior of globular proteins.^{25–28} The simulation of protein interactions^{29–31} can provide greater molecular resolution, but also point to some limitations of analysis in terms of two-particle interactions. One observation is that the spherically averaged interactions of proteins with net attraction may be dominated by attractive features between localized surface features in a small subset of relative orientations.^{32–34} While the osmotic second virial coefficient is often qualitatively correlated to the solution behavior of proteins, its values are not predictive of the type of phase transition for higher concentrations of a system or that of other protein molecules¹ suggesting limited utility of the two-particle interaction model to the behavior of concentrated systems where multiparticle interactions are expected. At high concentrations where molecular crowding affects both the range and the number of simultaneous interactions a protein molecule may experience, evaluation of protein interactions from SAXS and SANS structure factors also typically rely on pair potential functions. Such analysis generate “effective” pair potentials with the assumption of pairwise interaction additivity, a simplification which may overlook the role of different, more complex, simultaneous multiparticle interactions at higher concentrations. As one indication of multiparticle interaction effects, SAXS and SANS structure factor simulations often report protein–protein interaction parameters (effective pair potentials) that change with protein concentration.^{35–37} Currently, few approaches exist to characterize and understand the implications of more complex interactions in concentrated protein systems, but both condensed matter theory^{38,39} and experimental evidence from colloidal systems⁴⁰ support the importance of considering multiparticle interactions.

The use of light scattering methods to study multiparticle interactions of proteins was recently developed by Minton based on scaled particle theory to evaluate the effects of both molecular crowding and intermolecular interactions.⁴¹ Investigation of solution thermodynamics of MAbs at high concentrations with SLS offers a window to the solution behavior of molecules that represent a major vector of biopharmaceutical therapeutics. From a protein–colloidal physics perspective, MAbs also offer multidomain structural complexity and a large array of sequence variants accessible

with minimal changes to mAb secondary and tertiary structures. We recently described the ionic strength and concentration dependent behavior of an IgG1 monoclonal antibody (MAb1), shown to form transient clusters (self-associate) due in part to attractive, “patchy” electrostatic intermolecular interactions.⁴² Light scattering measurements, useful for gaining insights into solution protein–protein interactions, may also provide insights into the interactions between cosolutes and proteins.⁴³ In this contribution, we evaluate the interactions of MAb1 that lead to self-association at high concentrations with the pseudo two-component excess chemical potential as a function of protein concentration (1–235 mg/mL) and cosolute type. The hard sphere model of a single scattering species provided a basis for estimating mean intermolecular distances as a function of concentration and was also used to delineate mAb excluded volume contributions from interactions due to attractive or repulsive intermolecular forces. As a novel approach to understanding the role of many-particle interactions on protein solution nonideality at high concentrations, the excess chemical potential of MAb1 is evaluated as a function of mean interparticle distance. Modification of MAb1 solution light scattering and nonideality by NaCl, NaSCN, and arginine-chloride (Arg-Cl) was explored in a cosolute concentration (20–600 mM) dependent manner. The effects of NaCl, NaSCN, and Arg-Cl on MAb1 excess chemical potential are evaluated, with cosolutes used as probes of the weak, nonspecific intermolecular forces contributing to MAb1 interactions.

MATERIALS AND METHODS

MAb1 is a humanized monoclonal antibody based on an IgG1 framework with κ -light chains with an isoelectric point of 7.8, a total of 269 charged residues, and theoretical net charge of +17 at pH 6.0 based on fixed pK_a values for amino acid side chains. This molecule has been studied extensively over the years as a result of its interesting rheological and phase behavior.^{22,23,44–48} As with many monoclonal antibodies, this protein was expressed in Chinese hamster ovarian (CHO) cell lines, and purified by a series of chromatography steps, including affinity and ion exchange chromatography methods. The purified antibody was obtained as a concentrated solution from tangential flow filtration with added solution buffers and stabilizers, with MAb1 at 196 mg/mL.

Stock mAb starting materials were stored at 2–8 °C until further use. Additional preparation of mAb solutions included dialysis using Spectrapore 6–8 kD MWCO membrane (Spectrum Laboratories, CA). Approximately 50–60 mL stock solutions were dialyzed against 1.2 L of low ionic strength buffer containing 10 or 30 mM histidine-HCl at pH 6.0 over 48 h for a minimum of 3 times at 2–8 °C. The dialyzed mAb solutions were filtered through 0.22 μ m PVDF filters (Millipore Steriflip, Millipore Corp., MA) to remove any particulates. Typically, mAb concentrations of 140–150 mg/mL after dialysis were obtained. To obtain the higher mAb concentrations, 10 mL of mAb in 30 mM histidine-HCl, pH 6.0 were concentrated with Amicon YM30 Centriprep (Millipore Corp, MA) concentrators centrifuged at 2700 rpm. Final mAb concentrations in the dialyzed and centrifugally concentrated preparations were determined by using gravimetric dilutions and an absorptivity at 280 nm (A_{280}) of 1.6 (mg/mL) cm^{−1} for MAb1. The extinction coefficient was determined by quantitative amino acid analysis. Deionized water from a Milli-Q Biocel purification system with a 0.22 μ m filter was

used for all aqueous solution preparations. All buffers and reagents used were analytical grade or higher purity. All buffer solutions were titrated to the correct pH and filtered using Millipore Stericup GV 0.22 μm filters.

All mAb solutions used for light scattering experiments were prepared in 20 mL scintillation vials at 0.5–235 mg/mL by gravimetric dilution of known stock solution concentrations in a laminar flow hood. All scintillation vials were carefully cleaned with deionized water and dried in a stream of filtered compressed nitrogen gas prior to use. Stock solution concentrations were determined by gravimetric dilution to approximately 0.5 mg/mL and measurement of UV absorption at 280 nm using an Agilent diode array Spectrophotometer model 8453 with a 1 cm path length quartz cuvette. Before addition to protein solutions, all buffer and reagent solutions were additionally filtered through 0.10 μm Whatman Anotop 25 filters. After preparation or dilution of the samples, mAb solutions were briefly mixed by rotational agitation, and allowed to reach thermal and chemical equilibrium at controlled room temperature for 2 h. Protein solutions were centrifuged at room temperature for 20–30 min at 3000 rpm to remove adventitious dust and bubbles from the bulk of the solutions used for light scattering analysis. The highest concentration solutions (mAb > 170 mg/mL) were centrifuged for greater lengths of time until the light scattering signal showed a minimum of noise. Exterior surfaces of scintillation vials were lightly coated with low viscosity silicone oil to reduce undesired scattering from vial surface defects. Samples prepared as described above were directly placed in the beam of the light scattering instrument for measurements. By size exclusion chromatography, the stock MAb1 materials consisted of >98% monomer analyzed in dilute solution (1 mg/mL). Starting solutions of MAb1 in 30 mM histidine-HCl at pH 6.0 were derived from separate dialysis preparations showed highly similar concentration dependence of M_{wApp} . Sodium chloride (4.0 M), sodium thiocyanate (2.0 M), and arginine chloride (2.5 M) were prepared and filtered with 0.2 μm PVDF membranes before storage at room temperature until use. These cosolutes were introduced into the mAb solutions after an additional 0.1 μm filtration with gravimetric measurement of initial and final mass and volumes adjusted to achieve the desired cosolute concentrations in each vial.

Static Light Scattering from Solutions of a Single Species. For a single scattering species at arbitrary concentration, the generalized equation for Rayleigh scattering intensity ($R(\theta, c)$)⁴⁹ reduces to the expression in eq 1. In this limiting case, which can be applied to systems of purified monodisperse molecules (e.g., many proteins), $R(\theta, c)$ is a function of the scattering angle θ , and w/v concentration c_2 , and is directly related to the mass of the scattering species (M), the molecular size through the radius of gyration, R_G , and solute interactions described by the virial coefficients A_2 , A_3 , and so on, as shown below.

$$\frac{Kc_2}{R(\theta, c)} = \frac{1}{M} [1 + 2A_2Mc_2 + 3A_3Mc_2^2 + \dots] \\ \left[1 + \frac{q^2R_G^2}{3} + \dots \right] \quad (1)$$

where

$$K = \frac{4\pi^2 n^2}{N_A \lambda_o^4} \left(\frac{dn}{dc} \right)^2 \quad q = \frac{4\pi n_o (\sin \theta / 2)}{\lambda_o}$$

The system constant K includes the solution refractive index (n),⁵⁰ the wavelength of incident light (λ_o), the refractive index increment of scattering solute (dn/dc), scattering vector (q) at scattering angle (θ), and Avogadro's number (N_A). In the limit of infinite dilution ($c_2 \rightarrow 0$) and the scattering vector q approaching 0, eq 1 yields the value of $1/M$. In practice, light scattering measurements are made at both finite concentrations and angles, extrapolating to one or both limiting conditions to obtain M , the absolute molecular mass of the scattering species. Since many of the measurements discussed herein are far outside the approximation of infinite dilution, we introduce the value of apparent molecular mass (M_{wApp}), obtained at concentration c_2 in the limit of $\theta \rightarrow 0$, with the virial expansion terms in the denominator of eq 2 accounting for the intermolecular interactions between identical scattering species.

$$\frac{R(\theta = 0, c)}{Kc_2} = M_{\text{wApp}} \\ = M \left[\frac{1}{[1 + 2A_2Mc_2 + 3A_3Mc_2^2 + \dots]} \right] \quad (2)$$

An 18-angle Dawn EOS light scattering detector with a 30 mW solid state laser ($\lambda = 690$ nm) from Wyatt Technology (Santa Barbara, CA) was used for all static light scattering measurements with a water-cooled Peltier temperature controller set at 23 °C. The instrument was calibrated with 99.9% toluene (chromatography grade). For a typical scintillation vial experiment, a detector gain setting of 1X was used for all photodiodes, at fixed angles of 38–148°. Procedures used to normalize the angular dependency of the photodiodes relative to the 90° detector were conducted at the end of each experiment, according to the description provided elsewhere.⁴² All Rayleigh light scattering measurements of MAb1 were made relative to the appropriate cosolute and buffer containing solution with independent solutions in separate vials. Measurement of static light scattering intensity was conducted as a function of mAb concentration from 0.5 to 235 mg/mL, and as a function of cosolute concentrations (0–600 mM). Scattering data for each sample/vial was collected over an interval of 5–10 min with a data collection frequency of 12 points/minute. Astra 4.90.07 Software (Wyatt Technology Corporation, Santa Barbara, CA) was used to acquire and process the static light scattering data, with a dn/dc value of 0.185 applied to calculations that could be exported as raw data. Further analysis and calculations with the exported results were conducted in Microsoft Excel, Origin v7.5, and MATLAB R14.

Osmotic Second Virial Coefficient Measurement. Second osmotic virial coefficients (A_2) and the antibody molecular mass (M) were determined from samples <10 mg/mL (usually 3–4 concentrations) and linear extrapolation to infinite dilution. Uncertainties are mainly from linear fitting error alone and do not represent A_2 measurement reproducibility. The osmotic second virial coefficients represent the net magnitude of the two-body interactions of a single species of scatterers.

Excess Chemical Potential of Protein in Solution. Zimm⁵¹ and Debye⁵² provided the first fundamental understanding of Rayleigh light scattering from macromolecules in

solutions as the solution refractive index variations due to concentration/composition fluctuations and density fluctuations. Subsequently, Kirkwood and Goldberg⁵³ and Stockmayer⁵⁴ derived equations for light scattering from multicomponent solutions containing up to three components, including solvent (component 1), macromolecule (2), and cosolute (3). The solution composition fluctuations result from the equilibrium osmotic work acting on the macromolecules,⁵² which can be related to the excess chemical potential of macromolecule in solution and the collective interactions between solution components. The expression for the Rayleigh scattering from multicomponent systems simplifies to the two-component equation in the limit of weak interactions between cosolute and macromolecule.⁵⁵

$$\frac{Kc_2}{R(\theta = 0, c)} = \frac{1}{M} \left[1 + \frac{c_2}{RT} \left(\frac{\partial \mu_2^{\text{ex}}}{\partial c_2} \right)_{T,p} \right] \quad (3)$$

In utilizing the two-component equation, cosolute effects are treated as part of the solvent matrix. However, this compromise also facilitates and expands its application to macromolecule (MAb1) concentrations that exceed the first order terms of solution nonideality for the multicomponent expression. By substituting the apparent molecular weight measured at protein (MAb1) concentration c_2 , a simple expression for the excess chemical potential as a function of protein or hard sphere concentration was obtained.

$$\frac{M}{M_{\text{wApp}}} - 1 = \frac{c_2}{RT} \left(\frac{\partial \mu_2^{\text{ex}}}{\partial c_2} \right) \quad (4)$$

The excess chemical potential (μ_2^{ex}) is the chemical potential of the protein in solution with reference to its standard state (ideal) chemical potential and represents the Gibbs free energy dependence on the number of molecules in the system.⁵⁶ Eq 5 restates the excess chemical potential as a function of concentration in the form of virial expansion terms, which are also directly related to the activity coefficient (solution nonideality).^{43,57} Thus, higher order virial coefficients (exceeding two particle interactions of A_2), which account for the nonideality from many-particle interactions in concentrated systems, are fully described by the excess chemical potential.

$$\begin{aligned} \frac{1}{RT} \left(\frac{\partial \mu_2^{\text{ex}}}{\partial c_2} \right) &= \frac{\partial \ln \gamma_2}{\partial c_2} \\ &= [2A_2 M + 3A_3 M c_2 + 4A_4 M c_2^2 + \dots] \end{aligned} \quad (5)$$

Single Species of Scattering Hard Spheres as Reference. Experimental results were compared to light scattering intensities calculated from the Percus-Yeck equation of osmotic compressibility for single species of hard spheres (HS)⁵⁷ and detailed previously. In previous light scattering investigations, weakly or noninteracting IgG1 MAbs in solution were found to be well approximated by a simple hard sphere particle (three-dimensional) model with radius $R = 4.37 \text{ nm}$.⁴² The representation of MAb1 equivalent HS scattering as a function of concentration provides a point of reference with which to qualitatively interpret SLS of MAbs. Use of a single species of HS is also consistent with the limiting case (a monodisperse population of scatterers) of eqs 1–5 to describe MAb1 solution nonideality. Utilizing this simple hard sphere representation of MAb1 in solution permits additional

interesting features of the system to be evaluated, including the concentration dependence of the mean interparticle distance.⁵⁸

The excess chemical potential for a system of single species of HS is calculated using the virial expansion equation for osmotic compressibility⁵⁷ where the term in the denominator is $Z(\varphi)$

$$\begin{aligned} M_{\text{wApp}} &= M/[1 + 8\varphi + 30\varphi^2 + 73.4\varphi^3 + 141.2\varphi^4 \\ &\quad + 238.5\varphi^5 + 395\varphi^6 + \dots] \end{aligned} \quad (6)$$

so that

$$\frac{\varphi}{RT} \left(\frac{\partial \mu_{\text{HS}}^{\text{ex}}}{\partial \varphi} \right) = Z(\varphi) - 1 \quad (7)$$

Volume fractions (φ) were calculated according to eq 8 for a given value for sphere-equivalent radius (R) using the molecular weight (M) for mAb $\approx 150 \text{ kDa}$, where c_2 is protein concentration in g/mL and N_A is $6.022 \times 10^{23} \text{ mol}^{-1}$:

$$\varphi = \left(\frac{4\pi R^3}{3M} \right) N_A c_2 \quad (8)$$

Based on the work of Torquato,⁵⁸ the mean nearest neighbor distance boundaries for an equilibrium system with ergodic, isotropic packing for hard particles of D dimensions ($D = 1$ rod, 2 discs, 3 spheres) may be calculated based on particle size and particle dimension number. Although IgG1 molecules are not spheres in solution based on their crystal structures and solution SAXS, any intermediate approximations of actual mAb shape are deferred for practical purposes here. A relationship between mAb concentration (c_2) and mean interparticle surface separation, $\langle r \rangle = 2R(\lambda - 1)$, can be established for noninteracting hard sphere species where λ has been defined as the mean distance between centers of mass for nearest neighbors obtained from a conditional pair distribution function.⁵⁸ The mean interparticle distance dependence on concentration (or volume fraction) $\langle r(c) \rangle$ was calculated for given effective hard sphere radii (R) values, solved graphically to obtain $(dc_2/d\langle r \rangle)$, and used to transform the expression for excess chemical potential of a two component system into a function of $\langle r \rangle$.

$$\frac{M}{M_{\text{wApp}}} - 1 = \frac{\langle r(c_2) \rangle}{RT} \left(\frac{\partial \mu_2^{\text{ex}}}{\partial c_2} \right) \left(\frac{\partial c_2}{\partial \langle r \rangle} \right) = \frac{\langle r \rangle}{RT} \left(\frac{\partial \mu_2^{\text{ex}}}{\partial \langle r \rangle} \right) \quad (9)$$

The excess chemical potential of protein solutions consists of contributions from repulsive excluded volume effects, as well as contributions from the net intermolecular attractive and repulsive interactions. To interpret the underlying intermolecular interactions between MAbs, contributions to the excess chemical potential were delineated as the difference ($\Delta\mu_2^{\text{ex}}$) between measured net interactions and contributions from the hard sphere reference system.⁵⁹

$$\Delta\mu_2^{\text{ex}} = \mu_2^{\text{ex}} - \mu_{\text{HS}}^{\text{ex}} \quad (10)$$

Surface Electrostatic and Hydrophobicity Mapping. A homology model of MAb1 was generated using Modeller9v7 software and the crystal structure coordinates of anti-Her2 (PDBs 3D6G and 3N8S).⁶⁰ The electrostatic surface of the MAb1 model was calculated using the Adaptive Poisson–Boltzmann Solver version 1.3 (APBS).⁶¹ The electrostatic

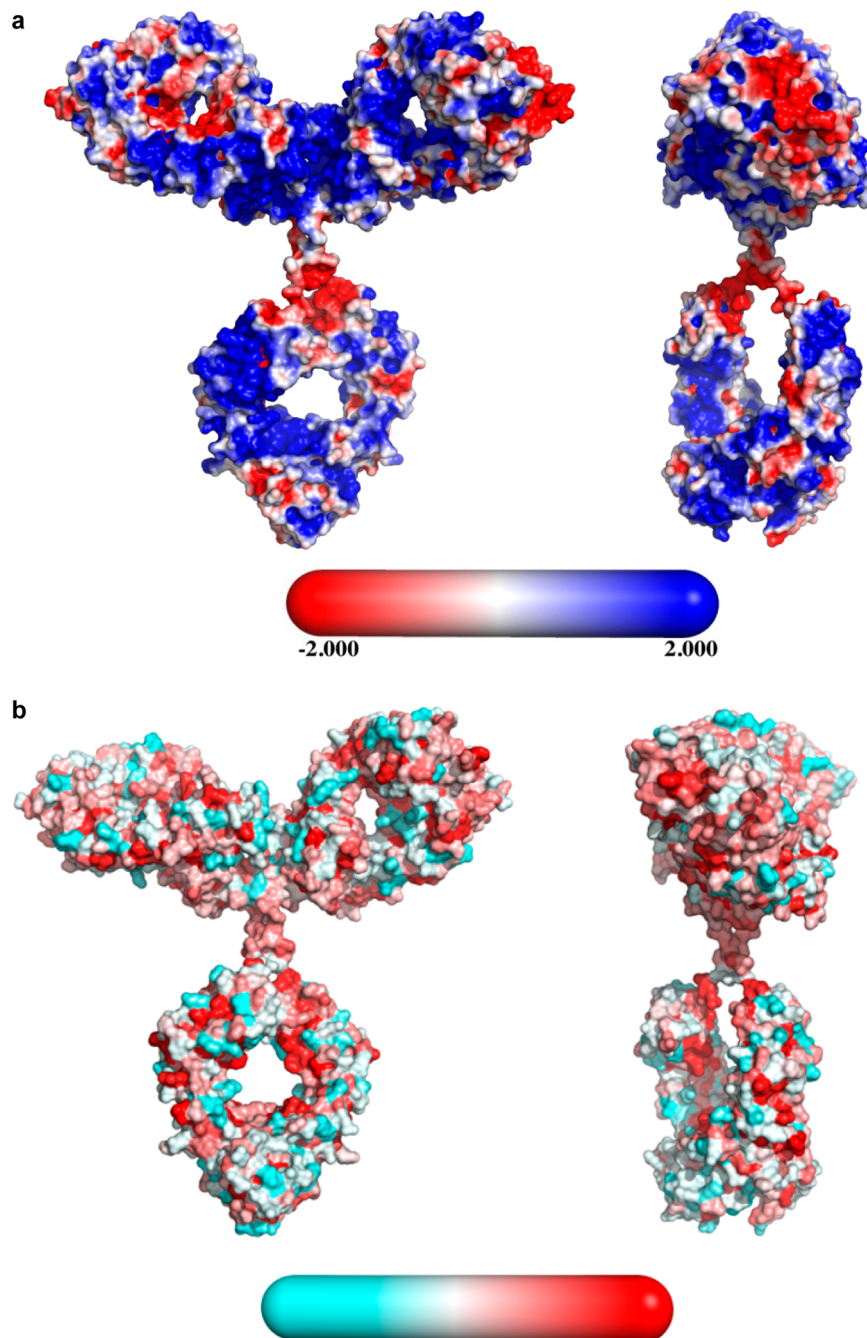


Figure 1. (a, b) Surface charge density map for MAb1 calculated with PyMol and PropKa using AMBER force field at pH 6.0. A negatively charged patch (red) appears in the CDR of the Fab (top, side view) and a number of positively charged surface patches (blue) are evident on both Fabs and the Fc portions of the molecule (a). Hydrophobic surface map of the MAb1 calculated from the same structure file (b) shown bottom, with front and side facing view, with more hydrophobic surface features shown in red.

surface charge distribution of MAb1 was calculated with a linearized Poisson–Boltzmann (PB) equation and cubic B-spline discretization of the charge distributions. Hydrophobic surfaces were calculated with a Pymol visualization script (`color_h`) utilizing the Eisenberg normalized consensus hydrophobicity scale.⁶² The resulting electrostatic and hydrophobic surfaces were visualized by PyMoL (Schrodinger LLC, San Diego, CA).

RESULTS AND DISCUSSION

Molecular Surface Features of MAb1. Static light scattering experiments with MAb1 previously highlighted the

important contributions of attractive electrostatic interactions and excluded volume effects to protein interactions at high concentrations and examined the thermodynamics of self-association behavior of MAb1 with both simple noninteracting HS and multiple species of interacting HS models.⁴² The attractive interactions of MAb1 lead to reversible formation of oligomeric species (transient clusters) as a function of salt concentration. The origin of the electrostatic attractive interactions has been previously attributed to MAb1 surface charge heterogeneity^{22,42} and was explored through the solution rheology of amino acid point mutation variants.⁴⁸ More recently, direct evidence of the surface charge

heterogeneity of MAbs and its role in anomalous solution behavior was established through chemical labeling and MS characterization with a related IgG1 molecule.⁶³ Figure 1a illustrates the localized regions or patches of surface charge at pH 6.0 for MAb1 calculated with PyMol. A negatively charged patch in the CDR of the Fab, produced by the tertiary structure grouping of four aspartic acid residues and one glutamic acid residue, and a number of positively charged patches over the surface of both Fabs and Fc regions of the mAb provide ample complementary structural features for attractive electrostatic interactions. A hydrophobic surface map of the molecule (Figure 1b) provides a similar map of hydrophobic surface heterogeneity, however with fewer easily identifiable features of potential importance. Here, the objective was to present a novel approach to interpreting the thermodynamic equilibrium chemical potential and colloidal interactions of MAb1 at high concentrations, and to probe the types of intermolecular protein interactions present through the use of different cosolutes over a range of cosolute concentrations.

Solution Apparent Molecular Weight versus Concentration. Considering the solution to consist of a single species of interacting MAb1 molecules, we utilize the chemical potential of the protein (for the pseudo-two-component system) and a hard sphere reference system to determine the effects of NaSCN, arginine-HCl and NaCl on the interactions of MAb1. Thus, the present manuscript treats the mAb interactions as a solution of monodisperse particles that interact weakly through nonspecific attractive intermolecular interactions and excluded volume repulsion. It is worth noting that this treatment of mAb interactions is conceptually compatible with the formation of transient protein clusters at equilibrium (self-associated states, as reported previously).⁴² The reversible formation of protein clusters or self-associated states result from simultaneous temporary interactions between a number of individual particles/mAb monomers. Such interactions become increasingly frequent in occurrence and prevalent at higher concentrations. The concentration fluctuations and interactions are measured as time-averaged equilibrium phenomena by SLS, and therefore, the question of “interacting species” or “associated states” of particles or protein molecules is one and the same when the interactions are reversible and nonspecific.

Generally, we observed that MAb1 solutions did not scatter light with strong angular dependency. The isotropic scattering intensity as a function of angle confirms that no large irreversible aggregates were present or being formed at the concentrations used in the samples. The apparent molecular weight obtained for solutions are shown as a function of MAb1 concentration in Figure 2a–c for solutions with 0–600 mM added NaCl (Figure 2a), NaSCN (Figure 2b), and Arg-Cl (Figure 2c). These data form the basis of all subsequent analysis, with several similarities between the three experiments with NaCl, NaSCN, and Arg-Cl solutions of MAb1. The obvious nonlinearity of the M_{wApp} versus concentration profiles represents competing effects of protein self-association and volume exclusion on intermolecular interactions, spatial distributions and concentration fluctuations. At lower Mab1 concentrations (1–50 mg/mL) and cosolute levels of 20–100 mM, M_{wApp} values generally increased as a function of protein concentration, a hallmark of attractive two-particle intermolecular interactions and the occurrence of reversible self-association. For MAb1 concentrations exceeding 50 g/mL,

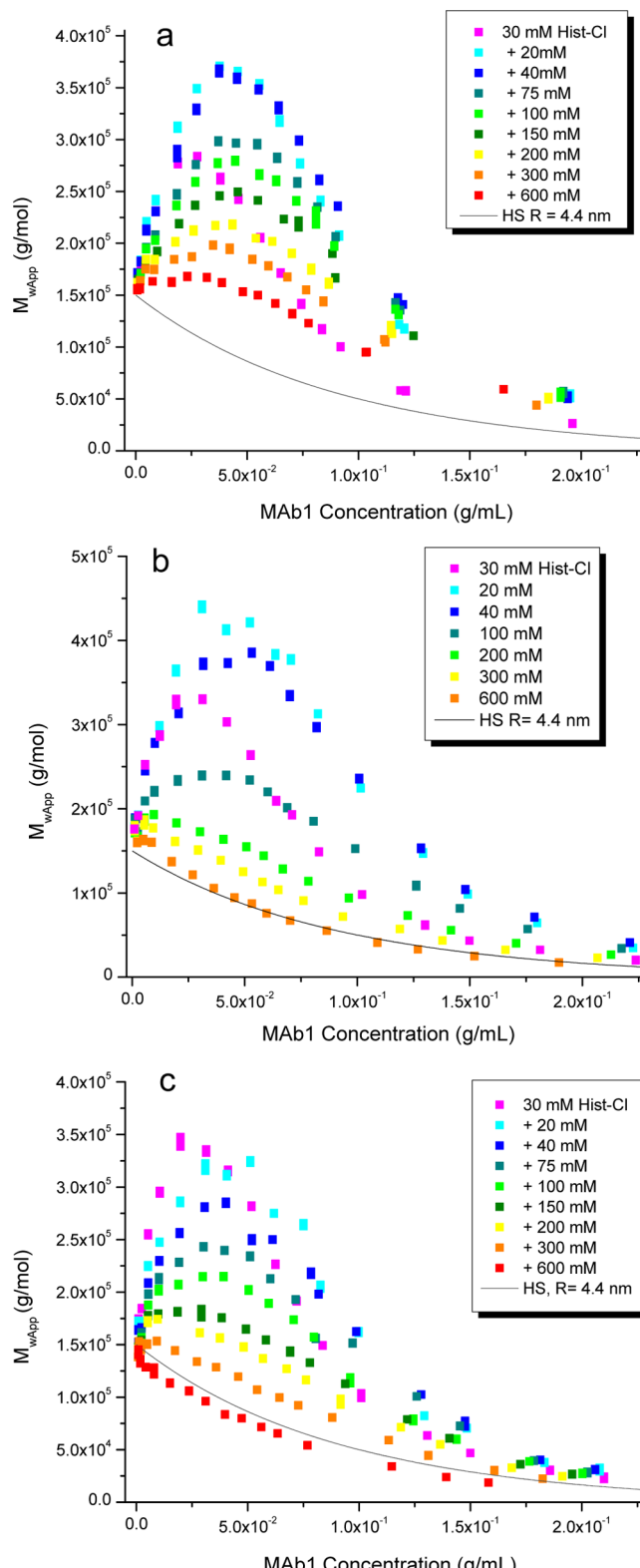


Figure 2. (a–c) Measured apparent molecular weight values as a function of MAb1 concentration in solutions with NaCl (a), NaSCN (b), and Arg-Cl (c) cosolute levels 0–0.6 M and pH = 6.0. The calculated M_{wApp} values for a single species of hard spheres (solid line) are shown for comparison.

M_{wApp} subsequently decreased with increasing concentration with all three cosolute systems, a feature attributable to the excluded volume of the mAb.⁴² Relative to the starting

solutions (buffered with 30 mM histidine-HCl), the addition of 20 mM NaCl and NaSCN was observed to shift the M_{wApp} maximum to higher concentration, increased the highest M_{wApp} values obtained, and generally appears to modify the concentration-dependent M_{wApp} profile. This effect is observed for initial increases in salt as well as histidine-HCl buffer concentrations (data not shown), suggesting that specific ion binding events may occur at low cosolute levels which negate some interactions or amplify the effect of other anisotropic interactions when the surface charge heterogeneity is perturbed. Increasing cosolute concentrations from 20 to 600 mM resulted in consistent decreases of the M_{wApp} values (at fixed mAb concentrations) across the MAb1 concentration range, but to distinctly different extents for NaCl, NaSCN, and Arg-Cl. This observation clearly indicates that the cosolutes can have different roles in reducing the attractive intermolecular interactions of MAb1 at pH 6. Calculated M_{wApp} for a single species of scattering HS ($R = \sim 4.4$ nm) obtained using the Carnahan–Starling expression for osmotic compressibility are compared as a reference system of noninteracting, self-avoiding particles for MAb1 in these cosolute systems. This HS radius corresponds to a volume of ~ 350 nm 3 that accounts not only for the mAb molar volume (182 nm 3) but also contributions from protein hydration and the effect of IgG1 shape on the excluded volume.

Quantitative results from the dilute regime of light scattering experiments in Supporting Information, Table S-1, summarize the molar mass obtained in the limit of infinite dilution (M) and the osmotic second virial coefficients (A_2) determined from concentrations of 1–10 mg/mL for each cosolute system. A_2 values are clearly negative at low ionic strength, but increased with added salts to values of -0.22 to 0.76×10^{-4} mol mL g $^{-2}$ at 600 mM cosolute levels. In Figure 3, A_2 values increased for

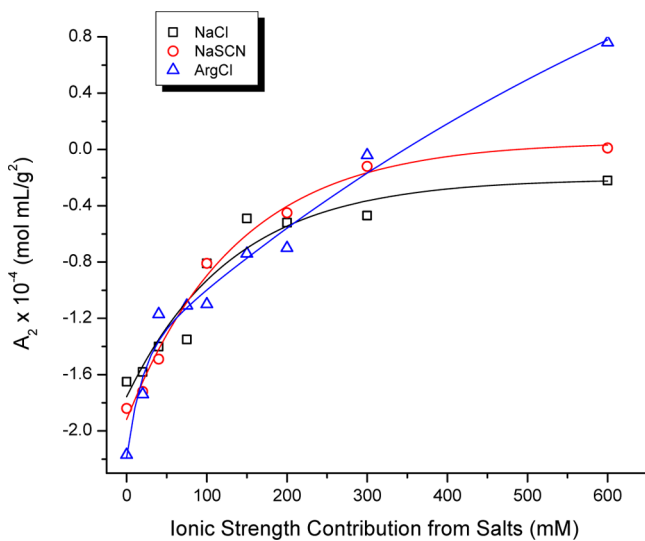


Figure 3. Osmotic second virial coefficients (obtained from the data in Figure 2) as a function of the ionic strength contributed by NaCl, NaSCN, and Arg-Cl cosolutes.

the three cosolute systems in a similar fashion until differentiation at the highest concentrations of salts, reflecting a weak dependence of protein–protein interactions in dilute solutions on cosolute specific effects. Molar mass values at infinite dilution (M) obtained as a function of cosolute show some variability (expected, based on the limited number (3–4) of

concentrations used), but these results confirm that the solutions consisted of monomeric mAb species and that the molecular interactions attributed to self-association are reversible. It is also important to note that M values did not show a strong dependency on cosolute concentrations, indicating that the interactions of cosolutes with MAb1 are in fact quite weak. These results contrast to polymer–cosolvent or highly charged polyelectrolyte-salt systems, where strong preferential cosolute–macromolecule interactions may affect the molar mass values obtained due to cosolute modification of the refractive index increment for the scattering species.^{53,64} The small or uncorrelated changes of MAb1 mass at infinite dilution indicate that the interactions of NaCl, NaSCN, and Arg-Cl with MAb1 are weak in nature. The weak interactions of NaCl, NaSCN, and Arg-Cl with MAb1 as a colloid/polyelectrolyte in tertiary solutions demonstrate that the simplified treatment of these systems as two component solutions is a reasonable approximation for interpreting the excess chemical potential of MAb1. Thus, the cosolutes are treated as part of the solvent matrix but are recognized as the modifying components of the matrix when differences between solution protein–protein interactions become evident.

Protein Excess Chemical Potential and Solution Nonideality.

Using eqs 3 and 4, the measured quantities from light scattering as a function of MAb1 concentration can be restated as the excess chemical potential of the protein (μ_2^{ex}) in the solution (Figure S-1). As a fundamental thermodynamic quantity of the system, the excess chemical potential defies simple characterization by statistical mechanical integrals of pair correlation functions beyond the first order correction to solution nonideality, A_2 .⁵⁶ Higher order terms of solution nonideality which account for multiparticle interactions currently remain challenging to describe with analytical forms of potentials of average force. However, use of the excess chemical potential as a function of solute concentration permits evaluation with a continuous set of expanding interactions both in terms of the numbers of interacting particles via the virial terms as seen in eq 5 and the underlying contributions of molecular forces. Previous work has demonstrated that higher order nonideality (multiparticle interaction) terms are required for interpretation of protein interactions in crowded conditions.^{41,42,65}

A relationship between mAb concentration (c_2) and mean interparticle surface separation calculated $\langle r \rangle$ isotropic, ergodic, noninteracting hard sphere species was calculated from a conditional pair distribution function.⁵⁸ In previous light scattering investigations, weakly or noninteracting IgG1 MAbs in solution were found to be well approximated by a hard sphere ($D = 3$) model in the limit of $\theta \rightarrow 0$, with radius $R \sim 4.4$ nm.⁴² This single species HS model for MAb1 was also used to calculate volume fraction and concentration dependence of mean interparticle distance $\langle r(c_2) \rangle$ for noninteracting mAb species. Figure 4 shows the calculated relationship between interparticle distance and bulk concentration for disk ($D = 2$), ellipse-like (approximated by $D = 2.5$), and spherical hard particles ($D = 3$) with radius $R = 4.37$ nm. A simpler, but less accurate calculation of interparticle distance which estimates the distance dependence based on the particle volume is also shown for comparison. Although the true shape of an antibody is not that of a disk, ellipsoid, or sphere, the distance dependence of the HS ($D = 3$) was utilized to estimate the average distances between nearest neighbor mAb particles and

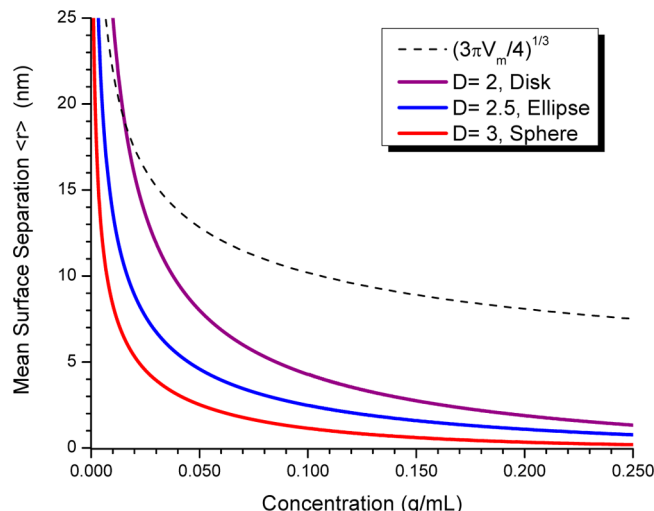


Figure 4. Mean intermolecular distances as a function of particle (assuming $R \sim 4.4$ nm) concentration for several potential models of MAb1 shape and excluded volume.

to remain consistent with the effective HS model used for mAb excluded volume interactions.

By using graphical analysis of the relationship between mean interparticle distances $\langle r \rangle$ as a function of known MAb1 concentration to obtain $d\mu_2^{\text{ex}}/d\langle r \rangle$, the excess chemical potential of a two component system can also be expressed as a function of $\langle r \rangle$ (eq 9). The representation of protein chemical potential obtained from light scattering as a function of mean intermolecular distance represents a new approach to interpreting the intermolecular interactions of proteins at high concentrations. Figure 5a–c shows the excess chemical potential of MAb1 solutions with NaCl, NaSCN, and Arg-Cl cosolutes at 20, 100, 300, and 600 mM (a subset of available data, reduced for clarity of presentation). To serve as a reference point, the excess chemical potential function of a system of noninteracting HS particles is also shown in each figure. At low solution ionic strengths the MAb1 chemical potentials μ_2^{ex} as a function of $\langle r \rangle$ take on the familiar form of a Lennard-Jones attractive intermolecular potential function.⁶⁶ Increasing the solution ionic strength generally reduced the well depth of the attractive interactions of MAb1.

Although a relationship between μ_2^{ex} and $\langle r \rangle$ is not treated in statistical thermodynamic theory, the derivation of the mean distance between nearest neighbors for an equilibrium egodic, isotropic ensemble is based on the equation of state for hard spheres.⁵⁸ This provides a linkage between the representation of $d\mu_2^{\text{ex}}/d\langle r \rangle$ and solution thermodynamics. Fundamentally, the concentration fluctuations that give rise to light scattering are the result of thermodynamic work of the system. The mean interparticle distance $\langle r \rangle$ represents the average distance between noninteracting HS particles determined by volume exclusion but does not reflect the deviations from the mean that attractive protein interactions observed by Rayleigh light scattering imply. The deviation from average time and distance dependence of protein behavior in solution is obtained as scattered light intensity/chemical potential of MAb1 in the solution. Another important distinction is that the potential of mean interparticle distance $d\mu_2^{\text{ex}}/d\langle r \rangle$ describes the sum of all intermolecular interactions (eq 5) and does not represent the potential of mean force for two particle interactions defined by statistical mechanical theory for dilute solutions. As a result, the

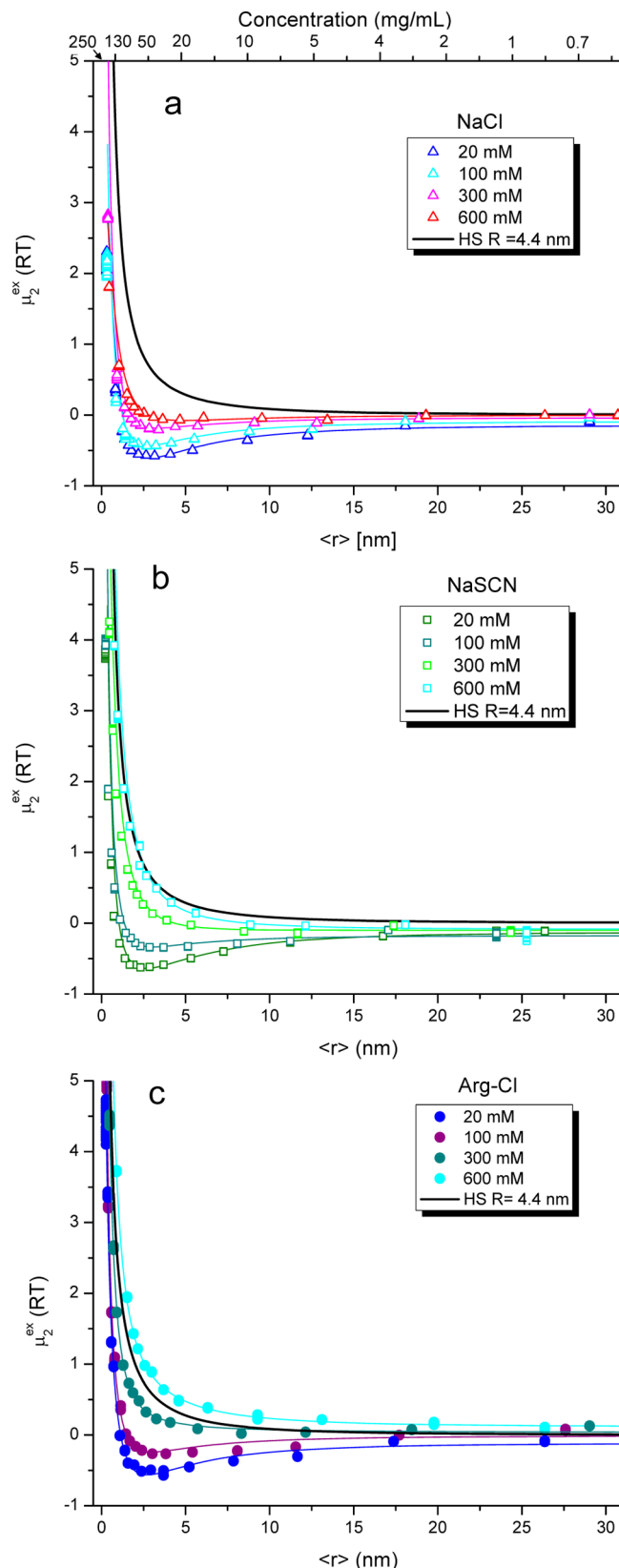


Figure 5. (a–c) Excess chemical potential of MAb1 solutions with NaCl (a), NaSCN (b), and Arg-Cl (c) at 20, 100, 300, and 600 mM represented as a function of mean intermolecular distance $\langle r \rangle$ for hard spheres. The lines accompanying the measured data were obtained from polynomial fits of MAb1 osmotic compressibility as a function of concentration.

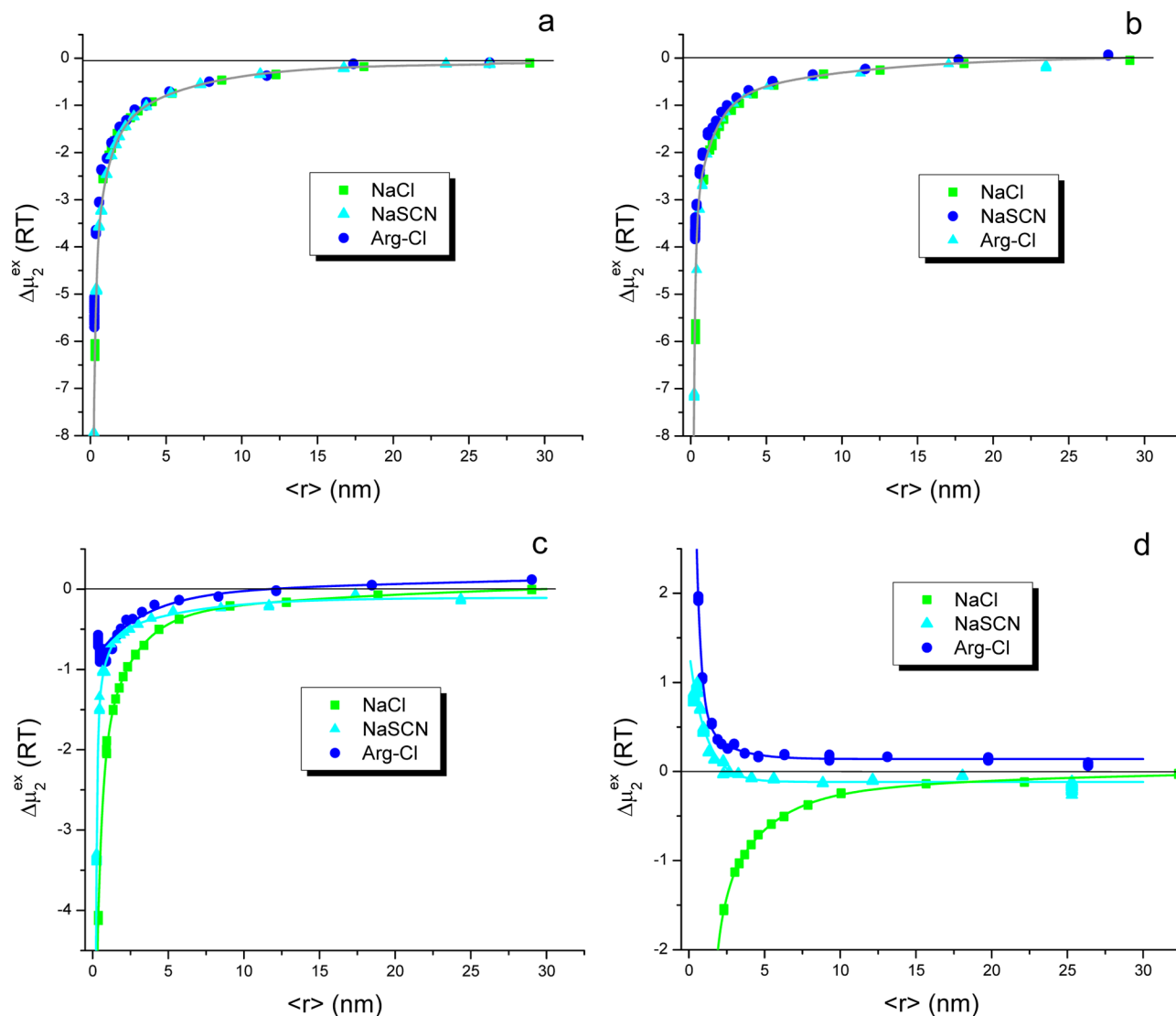


Figure 6. (a–d) Residual excess chemical potential of MAb1 solutions ($\Delta\mu_2^{\text{ex}}$) with NaCl, NaSCN, and Arg-Cl at 20 (a), 100 (b), 300 (c), and 600 mM (d) as a function of mean intermolecular distance $\langle r \rangle$. Lines in (a) and (b) represent concatenate fit results for all three data sets, while lines in (c) and (d) represent exponential function fit results for individual data sets. Removal of excluded volume effects from the measured MAb1 excess chemical potentials reveals the underlying intermolecular interactions, in particular, the multiparticle attractive interactions that are amplified at small separation distances.

$d\mu_2^{\text{ex}}/d\langle r \rangle$ function does not require the assumption of pairwise additivity to represent the net effects of many particle interactions that occur at high concentrations. A simple, but more accurate, conceptual interpretation is that the excess chemical potential functions in Figure 5a–c represent the work required to add another particle to the system⁵⁶ (at the cosolute levels and conditions of the experiment) when the particles of the system are separated by a mean distance $\langle r \rangle$. These results are relevant to the process of sequential molecule/particle addition and provide an experimental description of this process for high concentration mAb solutions.

Considering the excess chemical potential of protein solutions as series of sequential additions of molecules provides an estimation of the strength of intermolecular interactions as a function of intermolecular distance, as well as the contributions and range of intermolecular forces. Precedence for this approach can be found in the investigations of colloidal interactions with osmotic stress measurements.^{67–70} By

analogy, characterization of MAb1 net interactions in solution as a function of $\langle r \rangle$ should permit some qualitative interpretation of the range and factors contributing to self-association. In the case of MAb1, both the negative second virial coefficient values in dilute solutions in Figure 3 and the weakly negative μ_2^{ex} in Figure 5 show that the attractive interactions appear to be longer range in solutions with low ionic strength and pH of 6.0, consistent with intermolecular interactions influenced by attractive electrostatic features (see Figure 1).

As MAb1 solutions become more concentrated and mean intermolecular distances smaller, the net interactions display a minima at $\langle r \rangle = 2.5$ –4 nm, beyond which they become positive and strongly repulsive (for $\langle r \rangle \sim 1$ nm) due to the increasing contributions of volume exclusion. In low ionic strength solutions the minimum μ_2^{ex} observed ranges from -0.4 to -0.6 RT. The μ_2^{ex} minima disappear as MAb1 attractive interactions are increasingly screened by the solution ionic strength at higher cosolute concentrations. At cosolute levels of 0.3–0.6 M,

effects on MAb1 interactions specific to the cosolute identity become apparent. These differences are evident in Figure 5a–c, but the degree of the effects of salt concentration and salt type are most readily compared in the absence of excluded volume (HS) contributions. By subtracting the calculated HS excess chemical potential from the measured chemical potential (eq 10), the underlying effects of molecular forces on the intermolecular interactions between protein molecules can be identified.^{59,71} With volume exclusion effects removed, $\Delta\mu_2^{\text{ex}}$ versus $\langle r \rangle$ functions in Figure 6a–d distinguish contributions to the excess chemical potential from other intermolecular interactions present and, in the case of MAb1, their dependence on cosolute concentration. The broader applicability of this analysis of high concentration interactions to other protein/colloidal systems (e.g., lysozyme) is established in Supporting Information, Figure S-2. Interpreting the protein solution nonideality using this approach provides several insights into the nature of protein interactions in crowded systems. First, even when the excess chemical potential of a protein/colloid is positive (indicating net repulsive interactions between molecules) due to the dominant contribution of volume exclusion to solution nonideality, attractive intermolecular interactions may be present that can affect the solution or colloidal suspension behavior. This is clearly illustrated by the difference chemical potential $\Delta\mu_2^{\text{ex}}$ for MAb1 in Figures 6a–c and lysozyme in Figure S-2c. Additionally, the collective attractive interactions between MAb1 (or lysozyme) molecules are shown to gain in strength with increasingly negative values as mean distances between molecules become smaller and higher order nonideality terms contribute to protein solution light scattering. Evaluation of the hidden contributions to solution nonideality also provides evidence that the intermolecular attractions may be amplified by multiparticle (many-body) interactions at reduced interparticle distances, particularly for $\langle r \rangle$ less than the molecular spherical equivalent dimensions ($R \sim 4.4$ nm for MAb1, $R \sim 2$ nm for lysozyme).

Multiparticle (mAb) Interactions at High Concentrations. The premise that multiparticle or many-body interactions are both present and highly relevant to the behavior of protein solutions at even moderate concentrations can be readily evaluated. To help examine the extent of multiparticle interactions, the virial expansion equation for the HS osmotic compressibility $Z(\varphi)$ (eq 6) again provides a useful tool. Following from the McMillan-Mayer formulation of statistical thermodynamics, each B_n ($n = 2, 3, 4$, etc.) virial coefficient represents the contributions to nonideality from n -body interactions for a gas or a two-component solution. A straightforward numerical evaluation of contributions to the HS excess chemical potential from each virial coefficient term yields the extent of multiparticle or n -body interactions present as a function of HS concentration (or volume fraction), as shown in Figure S-3. Such representation in Figure S-3a shows that even for the minimal (mAb representative) case of a single, noninteracting hard sphere species ($R \sim 4.4$ nm), the solution/suspension behavior requires inclusion of many-body volume exclusion effects for all concentrations beyond 20 mg/mL or $\varphi \geq 0.024$ to accurately describe the chemical potential of the system. Initially the dominant term, two-particle interactions steadily decline in fractional contribution as the higher order 3, 4, 5, etc., n -body interactions sequentially increase their contributions to nonideality with greater volume fractions (Figure S-3b). As a function of intermolecular distance, many-body effects become increasingly important

particularly when mean distances of separation $\langle r \rangle$ become smaller than the molecular dimensions R (≤ 5 nm, in the case of MAb1) illustrated in Figure S-3c. Many-body interactions in HS systems are not explicit particle–particle contacts being formed but rather the result of volume exclusion forcing increased positional/temporal correlations between multiple local particles. As these correlations increase, the number and strength of attractive interactions between protein molecules increase also. The addition of attractive features to the HS model for colloidal behavior is expected to increase the number of interactions (computationally still difficult to assess), resulting in the known effect of more significant (in a time-averaged sense) reversible multiparticle interactions at lower concentrations. At high concentrations of particles/molecules where mean interparticle distances are small, the asymptotic decrease of $\Delta\mu_2^{\text{ex}}$ as a function of $\langle r \rangle$ in Figures 6a–c and S-2c suggest increased many-body interactions couple with the attractive features of molecules to amplify the attractive interaction's net contribution to solution nonideality. The experimental determination of three-body interaction effects by Brunner et al. delineated the complex role of n -body effects even when two-body interactions are repulsive, observing a breakdown of pairwise interaction additivity and attractive contributions to the three-body interactions.⁴⁰ Recently described molecular simulations also show that correlated interactions may have a pronounced effect on the mean multiparticle interaction energies and CG-force fields.⁷² Speculatively, both the electrostatic attractive features and molecular anisotropy play a role in the relatively long ranged attractions⁴² and synergistic effects obtained from many-body MAb1 interactions. Simulations of colloidal systems incorporating particle shape asymmetry and anisotropic (directional) interactions are expected to yield additional insights into the confluence of many-body interactions, effective attraction strength, their distance dependence, and ultimately their impact on colloidal phase behavior.

Cosolute Specific Effects on MAb1 Chemical Potential and Interactions. In an effort to better understand attractive MAb1 interactions, cosolute additives were used to probe the molecular forces governing the self-association at high concentrations. The attractive interactions of MAb1, greatest at 20 mM cosolute levels, were incrementally mitigated by increasing cosolute (NaCl, NaSCN and Arg-Cl) concentrations. Figure 6a,b reveals that, at 20 and 100 mM levels, all three cosolutes have highly similar effects on MAb1 interactions and chemical potential in both concentrated and dilute (see Figure 3) protein solution regimes. From these results it is possible to conclude that lower concentrations of NaCl, NaSCN, and Arg-Cl primarily affect MAb1 solution behavior through the screening of electrostatic attractive interactions between MAb1 molecules.

With the addition of 0.3–0.6 M cosolutes, the $\Delta\mu_2^{\text{ex}}$ potential functions (Figure 6c,d) showed increasing and pronounced differences based on cosolute identity, suggesting cosolute specific effects on MAb1 interactions were observed. Furthermore, cosolute specific effects on MAb1 excess chemical potential evident at 0.3 M and at 0.6 M cosolute levels were most pronounced at small $\langle r \rangle$ or higher MAb1 concentrations. Most notably, MAb1 solutions with 0.6 M Arg-Cl had positive $\Delta\mu_2^{\text{ex}}$ signifying net repulsive interactions at all $\langle r \rangle$ and concentrations (Figure 6d). The fact that repulsive interactions exceeding HS contributions were observed in solutions with 0.6 M Arg-Cl (high ionic strength) is quite interesting and may

arise through a number of different potential mechanisms that could coincide with the elimination of attractive MAb1 interactions. In one such mechanism, the weak preferential exclusion of arginine results in the preferential hydration of MAb1 surfaces, effectively increasing the MAb1 excluded volume to produce weakly repulsive net interactions across the intermolecular distance/concentration range. An alternative explanation could be that the additional conformational flexibility derived from high Arg-Cl concentrations⁷³ also increases the effective excluded volume of MAb1. In contrast, the $\Delta\mu_2^{\text{ex}}$ of MAb1 solutions with 0.6 M NaCl remained negative, consistent with the presence of residual attractive interactions. Because the chloride anion is common to both Arg-Cl and NaCl cosolute systems, the differences in solution nonideality behavior and the remarkable impact of Arg-Cl (μ_2^{ex} and $\Delta\mu_2^{\text{ex}}$) can be attributed specifically to arginine–MAb1 interactions.

MAb1 interactions modified by 0.6 M (and to a lesser extent 0.3 M) NaSCN appear to be more complex: in concentrated solutions (short $\langle r \rangle$) $\Delta\mu_2^{\text{ex}}$ was positive and similar in range as the Arg-Cl case, while at greater distances of mean separation, $\Delta\mu_2^{\text{ex}}$ remained slightly negative and therefore weakly attractive. In comparison to the use of NaCl, which was only partially successful in regulating attractive interactions, NaSCN was found to principally mitigate the attractive many-body interactions at small $\langle r \rangle$, while arginine-HCl eliminated both the long-range and the many-body short-range contributions to the attractive interactions. The effects of both NaSCN and Arg-Cl at 0.6 M cosolute levels are consistent with the capacity of these cosolutes to engage in weak interactions with exposed hydrophobic interfaces in water.^{12,21,74,75} Evaluating the hydrophobicity surface map (Figure 1b), a hydrophobic region next to the negatively charged patch in the CDR can be speculatively identified. This patch, formed by two surface colocated tryptophan residues and a phenylalanine residue, may provide an additional solvent exposed and extended feature contributing hydrophobic aspects to the MAb1 self-association. Collectively, the reduction of attractive interactions at high MAb1 concentrations by Arg-Cl and NaSCN indicate that, while MAb1 self-association at high concentrations is primarily caused by attractive electrostatic interactions from oppositely charged patches, a secondary contribution from MAb1 hydrophobic interactions is also present.

Cosolute effects on protein–protein interactions can be quantified with the derivatives of protein chemical potential and cosolute concentration, $d\mu_2^{\text{ex}}/dC_3$. Accepting that molal quantities may be approximated with molar quantities (negligible differences over cosolute concentrations (C_3) used here), $d\mu_2^{\text{ex}}/dC_3$ is directly related to the thermodynamic transfer free energy for solute interactions $\Delta G_{\text{tr}}/m_3$.⁷⁶ Utilizing μ_2^{ex} for systems with 0.02, 0.1, 0.3, and 0.6 M cosolutes, $d\mu_2^{\text{ex}}/dC_3$ could be determined for fixed MAb1 concentrations (Supporting Information, Figure S-4). The resulting first order trends obtained for 5, 50, 125, 200, and 250 mg/mL MAb1, are summarized in Figure 7. The magnitudes of the cosolute effect on MAb1 self-interactions follow a rank ordering of Arg-Cl > NaSCN ≫ NaCl, although the transfer free energy $d\mu_2^{\text{ex}}/dC_3$ does not address the type or nature of the cosolute interactions with the surface of the protein. Despite this mechanistic ambiguity, a number of the cosolute effects on MAb1 interactions can be readily recognized. First, the influence of NaCl is weak and MAb1 concentration independent. Arg-Cl and NaSCN influences on $d\mu_2^{\text{ex}}/dC_3$ are larger and positive, and

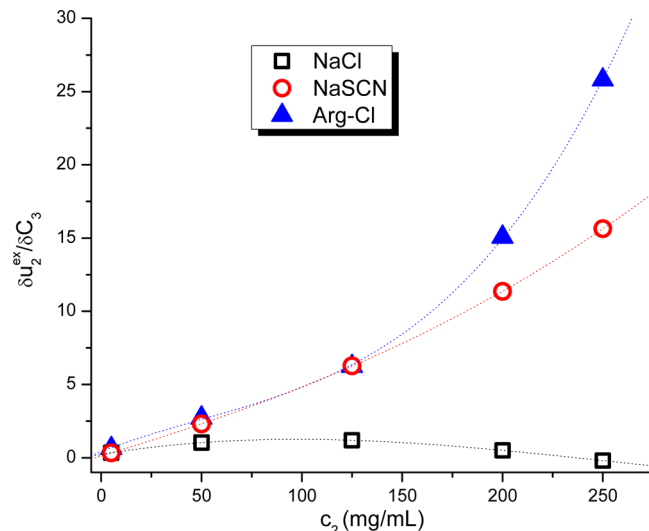


Figure 7. Chemical potential derivatives as a function of cosolute concentration, evaluated at several protein (MAb1) concentrations. The role of the cosolute becomes increasingly important to mitigating the interactions of MAb1 at higher protein concentrations.

suggest net preferential exclusion from the proximity of the IgG1 surface. Also shown in Figure 7 is that NaSCN and Arg-Cl modified MAb1 solution chemical potentials to similar extents up to concentrations of 125 mg/mL MAb1. Perhaps most interesting is the evident nonlinearity of $d\mu_2^{\text{ex}}/dC_3$ for Arg-Cl solutions at MAb1 concentrations >125 mg/mL, which may be due to a synergistic or specific role of Arg-Cl in disrupting some of the protein–protein interactions at high concentrations. Both NaSCN and Arg-Cl were especially effective in modifying the chemical potential of MAb1 solutions at high protein concentrations where multiparticle interactions and self-association are prevalent. The observations presented here shed new light on the role of many-body effects and cosolutes on protein–protein interactions at high concentrations. A more detailed analysis of the solution thermodynamics with respect to the specific and nonspecific cosolute–protein interactions that contribute to MAb1 solution behavior will be explored in a subsequent contribution.

CONCLUSIONS

While it is intuitive that when molecules become more concentrated the mean distances that separate them become smaller, it is not as widely recognized that their interactions also become more complex. As a new approach to interpreting the interactions of proteins at high concentrations, the excess chemical potential of a protein (MAb1) measured by static light scattering was analyzed as a function of calculated mean intermolecular distance. The representation of excess chemical potential μ_2^{ex} as a function of mean intermolecular distance, essentially the work of particle addition to a system of like particles, provides a new method for analyzing the net effects of solution nonideality caused by multiparticle interactions. Utilizing a simple hard sphere model representative of MAbs (or other proteins), the contributions of attractive intermolecular interactions can be distinguished from the repulsive excluded volume effect, which dominates the net solution interactions of proteins at high concentrations. The underlying $\Delta\mu_2^{\text{ex}}$ functions reveal that, as mean intermolecular distances become smaller than the dimensions of the protein, attractive

interactions are increasingly potent contributors to protein solution behavior, particularly through cooperative multiparticle interactions. Treatment of the protein excess chemical potential as a function of mean intermolecular distance is also shown to be generally applicable to other protein systems (e.g., lysozyme) at high concentrations.

MAb1 excess chemical potentials were modified by increasing levels of ionic cosolutes NaCl, NaSCN, and Arg-Cl, which were used to probe the molecular contributions to the reversible self-association of this particular antibody. All three cosolutes reduced MAb1 attractive interactions in an ionic strength dependent manner, screening electrostatic interactions due to oppositely charged patches. Cosecutive specific effects of NaSCN and Arg-Cl at $C_3 \geq 0.3$ M further decreased MAb1 attractive many-body interactions at high protein concentrations, indicating contributions from hydrophobic surface features as well. As the most effective solution additive evaluated, arginine was shown to have a functional role in the complete mitigation of MAb1 attractive intermolecular interactions in high concentration solutions. Arginine-Cl, it can be concluded from these experiments, has a hybrid role as a cosolute in mitigating both ionic and hydrophobic interactions between proteins.

Here a new approach has been proposed for the interpretation of protein interactions at high concentrations where simultaneous, multiparticle attractive interactions (equilibrium clustering) may manifest in anomalous solution behavior such as high viscosities, opalescence, liquid–liquid phase separation, gelation, and precipitation. The chemical potential as a function of mean intermolecular distance provides a new approach to understanding the volume fraction/density dependence function of colloidal interactions. Finally, in the absence of excluded volume contributions the excess chemical potential shows how attractive interactions and intermolecular interactions, in general, are amplified by many-body correlations at high concentrations. It is anticipated that these experimental results for the process of sequential molecule addition (or subtraction)⁷⁷ when combined with simulations may also promote a better theoretical understanding of multiparticle interactions present in a wide variety of technologically relevant colloidal systems.

■ ASSOCIATED CONTENT

Supporting Information

Detailed data on osmotic second virial coefficients and molecular weights obtained at infinite dilution are found in Table S-1. Figures S-1 and S-4 illustrate the analysis of the excess chemical potential as a function of cosolute concentration. Figure S-2 provides an analysis excess chemical potential as a function of mean separation for lysozyme. Figure S-3 illustrates the concentration and distance dependence of multibody interactions for a simple HS model consistent with the spherical equivalent dimensions of a mAb. This material is available free of charge via the Internet at <http://pubs.acs.org>.

■ AUTHOR INFORMATION

Corresponding Author

*E-mail: tscherer@gene.com.

Notes

The authors declare no competing financial interest.

■ ACKNOWLEDGMENTS

The author gratefully acknowledges Drs. Allen Minton, Daniel Some, and Steven Trainoff for insightful discussions. Drs. Kedar Dave and Wayne G. Lilyestrom are also acknowledged for assistance with calculations of mean interparticle distance functions and MAb1 electrostatic and hydrophobic surface representations, respectively.

■ REFERENCES

- (1) Lewus, R. A.; Darcy, P. A.; Lenhoff, A. M.; Sandler, S. I. *Biotechnol. Prog.* **2011**, *27*, 280–289.
- (2) Mason, B. D.; Zhang, L.; Remmeli, R. L.; Zhang, J. F. *J. Pharm. Sci.* **2011**, *100*, 4587–4596.
- (3) Wang, Y.; Lomakin, A.; Latypov, R. F.; Benedek, G. B. *Proc. Natl. Acad. Sci. U.S.A.* **2011**, *108*, 16606–16611.
- (4) Leckband, D.; Sivasankar, S. *Colloids Surf., B* **1999**, *14*, 83.
- (5) Kumar, S.; Nussinov, R. *ChemBioChem* **2002**, *3*, 604–617.
- (6) Leckband, D. E.; Schmitt, F. J.; Israelachvili, J. N.; Knoll, W. *Biochemistry* **1994**, *33*, 4611–4624.
- (7) Lesins, V.; Ruckenstein, E. *Colloid Polym. Sci.* **1988**, *266*, 1187–1190.
- (8) Pande, A.; Ghosh, K. S.; Banerjee, P. R.; Pande, J. *Biochemistry* **2010**, *49*, 6122–6129.
- (9) Auton, M.; Bolen, D. W.; Rosgen, J. *Proteins* **2008**, *73*, 802–813.
- (10) Curtis, R. A.; Ulrich, J.; Montaser, A.; Prausnitz, J. M.; Blanch, H. W. *Biotechnol. Bioeng.* **2002**, *79*, 367–380.
- (11) Piazza, R.; Pierno, M. *J. Phys.: Condens. Matter* **2000**, *12*, A443–A449.
- (12) Gibb, C. L. D.; Gibb, B. C. *J. Am. Chem. Soc.* **2011**, *133*, 7344–7347.
- (13) Boncina, M.; Lah, J.; Rescic, J.; Vlachy, V. *J. Phys. Chem. B* **2010**, *114*, 4313–4319.
- (14) Hess, B.; van der Vegt, N. F. A. *Proc. Natl. Acad. Sci. U.S.A.* **2009**, *106*, 13296–13300.
- (15) Collins, K. D. *Methods* **2004**, *34*, 300–311.
- (16) Pegram, L. M.; Record, M. T. *J. Phys. Chem. B* **2008**, *112*, 9428–9436.
- (17) Miao, L.; Qin, H.; Koehl, P.; Song, J. *FEBS Lett.* **2011**, *585*, 3126–3132.
- (18) Arakawa, T.; Ejima, D.; Tsumoto, K.; Obeyama, N.; Tanaka, Y.; Kita, Y.; Timasheff, S. N. *Biophys. Chem.* **2007**, *127*, 1–8.
- (19) Shukla, D.; Trout, B. L. *J. Phys. Chem. B* **2011**, *115*, 1243–1253.
- (20) Shukla, D.; Zamolo, L.; Cavallotti, C.; Trout, B. L. *J. Phys. Chem. B* **2011**, *115*, 2645–2654.
- (21) Ito, L.; Shiraki, K.; Matsuura, T.; Okumura, M.; Hasegawa, K.; Baba, S.; Yamaguchi, H.; Kumashita, T. *Protein Eng. Des. Sel.* **2011**, *24*, 269–274.
- (22) Liu, J.; Nguyen, M. D.; Andya, J. D.; Shire, S. J. *J. Pharm. Sci.* **2005**, *94*, 1928–1940.
- (23) Kanai, S.; Liu, J.; Patapoff, T. W.; Shire, S. J. *J. Pharm. Sci.* **2008**, *97*, 4219–4227.
- (24) Liu, J.; Shire, S. J. USPTO 7,666,413; Genentech Inc.: U.S.A., 2010, pp 1–33.
- (25) Chi, E. Y.; Krishnan, S.; Kendrick, B. S.; Chang, B. S.; Carpenter, J. F.; Randolph, T. W. *Protein Sci.* **2003**, *12*, 903–913.
- (26) Dumetz, A. C.; Chockla, A. M.; Kaler, E. W.; Lenhoff, A. M. *Biochim. Biophys. Acta, Proteins Proteomics* **2008**, *1784*, 600–610.
- (27) Dumetz, A. C.; Chockla, A. M.; Kaler, E. W.; Lenhoff, A. M. *Cryst. Growth Des.* **2009**, *9*, 682–691.
- (28) Dumetz, A. C.; Snellinger-O'Brien, A. M.; Kaler, E. W.; Lenhoff, A. M. *Protein Sci.* **2007**, *16*, 1867–1877.
- (29) Elcock, A. H.; McCammon, J. A. *Biophys. J.* **2001**, *80*, 613–625.
- (30) McGuffee, S. R.; Elcock, A. H. *J. Am. Chem. Soc.* **2006**, *128*, 12098–12110.
- (31) Asthagiri, D.; Neal, B. L.; Lenhoff, A. M. *Biophys. Chem.* **1999**, *78*, 219–231.
- (32) Persson, B. A.; Jonsson, B.; Lund, M. *J. Phys. Chem. B* **2009**, *113*, 10459–10464.

- (33) Neal, B. L.; Asthagiri, D.; Lenhoff, A. M. *Biophys. J.* **1998**, *75*, 2469–2477.
- (34) Hloucha, M.; Lodge, J. F. M.; Lenhoff, A. M.; Sandler, S. I. *J. Cryst. Growth* **2001**, *232*, 195–203.
- (35) Zhang, F.; Skoda, M. W. A.; Jacobs, R. M. J.; Martin, R. A.; Martin, C. M.; Schreiber, F. *J. Phys. Chem. B* **2007**, *111*, 251–259.
- (36) Liu, Y.; Porcar, L.; Chen, J.; Chen, W.-R.; Falus, P.; Faraone, A.; Fratini, E.; Hong, K.; Baglioni, P. *J. Phys. Chem. B* **2011**, *115*, 7238–7247.
- (37) Kim, S. J.; Dumont, C.; Gruebele, M. *Biophys. J.* **2008**, *94*, 4924–4931.
- (38) Lowen, H.; Allahyarov, E. *J. Phys.: Condens. Matter* **1998**, *10*, 4147–4160.
- (39) Dobnikar, J.; Brunner, M.; von Grunberg, H. H.; Bechinger, C. *Phys. Rev. E* **2004**, *69*–75.
- (40) Brunner, M.; Dobnikar, J.; von Grunberg, H. H.; Bechinger, C. *Phys. Rev. Lett.* **2004**, *92*, 078301–078305.
- (41) Minton, A. P. *Biophys. J.* **2007**, *93*, 1321–1328.
- (42) Scherer, T. M.; Liu, J.; Shire, S. J.; Minton, A. P. *J. Phys. Chem. B* **2010**, *114*, 12948–12957.
- (43) Eisenberg, H. *Biological Macromolecules and Polyelectrolytes in Solution*; Oxford University Press: London, 1976.
- (44) Kamerzell, T. J.; Kanai, S.; Liu, J.; Shire, S. J.; Wang, Y. *J. Phys. Chem. B* **2009**, *113*, 6109–6118.
- (45) Yadav, S.; Laue, T. M.; Kalonia, D. S.; Singh, S. N.; Shire, S. J. *Mol. Pharm.* **2012**, *9*, 791–802.
- (46) Yadav, S.; Liu, J.; Shire, S. J.; Kalonia, D. S. *J. Pharm. Sci.* **2009**, *99* (3), 1152–1168.
- (47) Yadav, S.; Scherer, T. M.; Shire, S. J.; Kalonia, D. S. *Anal. Biochem.* **2011**, *411*, 292–296.
- (48) Yadav, S.; Sreedhara, A.; Kanai, S.; Liu, J.; Lien, S.; Lowman, H.; Kalonia, D. S.; Shire, S. J. *Pharm. Res.* **2011**, *28*, 1750–1764.
- (49) Wyatt, P. *J. Anal. Chim. Acta* **1993**, *272*, 1–40.
- (50) Tanford, C. *The Physical Chemistry of Macromolecules*; John Wiley and Sons, Inc.: New York, 1961.
- (51) Zimm, B. H. *J. Chem. Phys.* **1945**, *13*, 141–145.
- (52) Debye, P. *J. Phys. Colloid Chem.* **1947**, *51*, 18–32.
- (53) Kirkwood, J. G.; Goldberg, R. J. *J. Chem. Phys.* **1950**, *18*, 54–57.
- (54) Stockmayer, W. H. *J. Chem. Phys.* **1950**, *18*, 58–61.
- (55) Timasheff, S. N.; Dintzis, H. M.; Kirkwood, J. G.; Coleman, B. D. *J. Am. Chem. Soc.* **1957**, *79*, 782–791.
- (56) Ben-Naim, A. *Statistical Thermodynamics for Chemists and Biochemists*; Plenum Press: New York, 1992.
- (57) Minton, A. P. *Methods in Enzymology*; Academic Press: New York, 1998; Vol. 295, pp 127–149.
- (58) Torquato, S. *Phys. Rev. Lett.* **1995**, *74*, 2156–2159.
- (59) Curtis, R. A.; Blanch, H. W.; Prausnitz, J. M. *J. Phys. Chem. B* **2001**, *105*, 2445–2452.
- (60) Eswar, N.; Marti-Renom, M. A.; Webb, B.; Madhusudhan, M. S.; Eremian, D.; Shen, M.; Pieper, U.; Sali, A. *Comparative Protein Structure Modeling with MODELLER*; John Wiley & Sons, Inc.: Hoboken, NJ, 2006; Vol. Supplement 15.
- (61) Baker, N. A.; Sept, D.; Joseph, S.; Holst, M. J.; McCammon, J. A. *Proc. Natl. Acad. Sci. U.S.A.* **2001**, *98*, 10037–10041.
- (62) Eisenberg, D.; Schwarz, E.; Komaromy, M.; Wall, R. *J. Mol. Biol.* **1984**, *179*, 125–142.
- (63) Zhang, L.; Lilyestrom, W.; Li, C.; Scherer, T.; van Reis, R.; Zhang, B. *Anal. Chem.* **2011**, *83*, 8501–8508.
- (64) Vrij, A.; Overbeek, J. T. G. *J. Colloid Sci.* **1962**, *17*, 570–588.
- (65) Fine, B. M.; Lomakin, A.; Ogun, O. O.; Benedek, G. B. *J. Chem. Phys.* **1996**, *104*, 326–335.
- (66) Israelachvili, J. N. *Intermolecular and Surface Forces*, 2nd ed.; Academic Press: San Diego, CA, 1991.
- (67) Barclay, L. M.; Ottewill, R. H. *Special Discuss. Faraday Soc.* **1970**, *138*–147.
- (68) Parsegian, V. A.; Rand, R. P.; Fuller, N. L.; Rau, D. C. *Methods Enzymol.* **1986**, *127*, 400–416.
- (69) Leneveu, D. M.; Rand, R. P.; Parsegian, V. A. *Nature* **1976**, *259*, 601–603.
- (70) Paineau, E.; Biannic, I.; Baravian, C.; Philippe, A.-M.; Davidson, P.; Levitz, P.; Funari, S. r. S.; Rochas, C.; Michot, L. J. *Langmuir* **2011**, *27*, 5562–5573.
- (71) Israelachvili, J.; Pashley, R. *Nature* **1982**, *300*, 341–342.
- (72) Rudzinski, J. F.; Noid, W. G. *J. Phys. Chem. B* **2012**, *116*, 8621–8635.
- (73) Lilyestrom, W. G.; Shire, S. J.; Scherer, T. M. *J. Phys. Chem. B* **2012**, *116*, 9611–9618.
- (74) Tadeo, X.; Pons, M.; Millet, O. *Biochemistry* **2007**, *46*, 917–923.
- (75) Schneider, C. P.; Trout, B. L. *J. Phys. Chem. B* **2009**, *113*, 2050–2058.
- (76) Timasheff, S. N. In *Protein Solvent Interactions*; Gregory, R. B., Ed.; Marcel Dekker: New York, 1995; pp 445–482.
- (77) Boulogeoris, G. C. *J. Phys. Chem. B* **2011**, *116*, 997–1006.